On the Use of Fourier Descriptors for the Assessment of Frequency Coupling Matrices of Power Electronic Devices

Roberto Langella
Alfredo Testa
Dept. of Ind. and Inf. Eng.
The University of Campania
Aversa, Italy
roberto.langella@unicampania.it

Joaquín E. Caicedo
Andrés A. Romero
Humberto C. Zini
Instituto de Energía Eléctrica
Univ. Nac. San Juan - CONICET
San Juan, Argentina
jcaicedo@iee.unsj.edu.ar

Jan Meyer
Dept. of El. Eng. and Inform.
Techn. Universitaet Dresden
Dresden, Germany
jan.meyer@tu-dresden.de

Neville R. Watson
Dept. of Elect. and Comp. Eng.
University of Canterbury
Christchurch, New Zealand
neville.watson@canterbury.ac.nz

***Abstract*— The use of Fourier descriptors (FD) for the assessment of frequency coupling matrices (FCM) of power electronic devices is considered. After some recalls on FDs, FCM approach is discussed showing how the matrices elements can be built basing on the use of maximum two FDs under linearity hypothesis. Then, a non-linearity index that allows to check the validity of the assumed "linearity hypothesis" and to quantify the obtainable accuracy is introduced. Numerical simulations on two very simple non linear circuits are performed to show the sensitivity of the FCM elements to magnitude and phase angle variation of the background harmonic distortion using FDs and the usefulness and the behavior of the non linearity index.**

***Index Terms*-- Frequency Coupling Matrices, Fourier Descriptors, Harmonics, Non-linear equipment, Power Quality.**

I. INTRODUCTION

FOURIER descriptors (FD) are commonly used in image recognition for the classification of closed looped objects [1], [2].

Frequency domain modeling of Power Electronic (PE) devices is a very commonly used approach to model the harmonic emission of modern power electronic devices in distribution networks [3], [4].

Frequency Coupling Matrices (FCM) are tools able to model the sensitivity of the current harmonic emission of PE devices to small deviations of the background voltage harmonics. They can be evaluated based on the assumption that power electronic device behavior around a suitable reference working point (e.g. ideal sinusoidal conditions) is linear for small variations from reference conditions (linearity hypothesis) [3], [5]. In [6], Smith *et al.* demonstrate the phase angle dependency of the FCM elements in HVDC converters. A similar behavior has been observed in single-phase power electronic devices [7], [8], such as Compact Fluorescent Lamps [9], [10] and LED lamps [11].

In [6], Smith *et al*. proposed a second rank tensor as a means of performing the nodal analysis of networks incorporating phase dependent impedance of a HVdc converter on the ac side. In order to minimize the sensitivity of the tensor parametrization to experimental errors and higher order complex non-linearities, in [8] the use of FDs to find the best tensor approximation to match the measured data was proposed. This intuition comes from the consideration that if the linearity hypothesis is verified the elements of the FCM describe a double circle locus on a complex plane as a function of the applied distortion angle.

In this paper, after some recalls on FDs, FCM approach is discussed and it is shown how the matrices elements can be built basing on the use of maximum two FDs under linearity hypothesis. Then, a non-linearity index (NLI) that allows to check the validity of the assumed "linearity hypothesis" and to quantify the obtainable accuracy is introduced. Numerical simulations on two very simple non linear circuits are performed to show the sensitivity of the FCM elements to magnitude and phase angle variation of the background harmonic distortion using FDs and the usefulness and the behavior of the non linearity index.

In a companion paper [12] the impact of reference working point on the frequency coupling matrix of a plug-in electric vehicle charger is analyzed using the NLI introduced in this paper.

II. FOURIER DESCRIPTORS

First some recalls about definition of FDs are given, then simple geometric patterns are described in terms of FDs.

A. Recalls

A closed looped oriented object in the complex plane can be represented by a sequence of complex numbers, $y(m_p)$, represented by means of M_p evenly spaced vectors as depicted in Figure 4. (a).

The Fourier descriptor is the discrete Fourier transform of the complex sequence, y, and is described by:

$$\underline{Y}_{fd}[n] = \frac{1}{M_p} \sum_{m_p=0}^{M_p-1} y(m_p) \cdot e^{jn\frac{2\pi m_p}{M_p}} \qquad (1)$$

where $\underline{Y}_{fd}[n]$ is the Fourier descriptor of order n. Each FD rotates at a rate which is proportional to its order multiplied by the unitary rate of change $\Theta = 2\pi \cdot m_p/M_p$.

Conversely, given the Fourier descriptors, the sequence can be reconstructed by the following equation:

$$y(m_p) = \sum_{n=-M_p/2}^{M_p/2} \underline{Y}_{fd}[n] \cdot e^{jn\Theta}. \qquad (2)$$

Figure 4. (b) shows the magnitudes and phase angles of the FD of the object shown in Figure 4. (a). versus the normalized frequency. Fig. 1 (c) depicts the reconstruction of the closed looped curve of Fig. 1 (a), based on the FDs.

The sum of the FDs, when $\Theta = 0$, *i.e.* $y(0)$, and the rate and direction of rotation of each vector, are represented. Each point of the curve is obtained by the sum of the rotating vectors. Note that, except $\underline{Y}_{fd}[0]$, all the FDs rotate. $\underline{Y}_{fd}[1]$, $\underline{Y}_{fd}[2]$, $\underline{Y}_{fd}[3]$ rotate at a rate of Θ, 2Θ, and 3Θ, respectively, in counterclockwise direction, whereas $\underline{Y}_{fd}[-3]$, and $\underline{Y}_{fd}[-2]$ rotate at a rate of 3Θ, and 2Θ, respectively, in the clockwise direction.

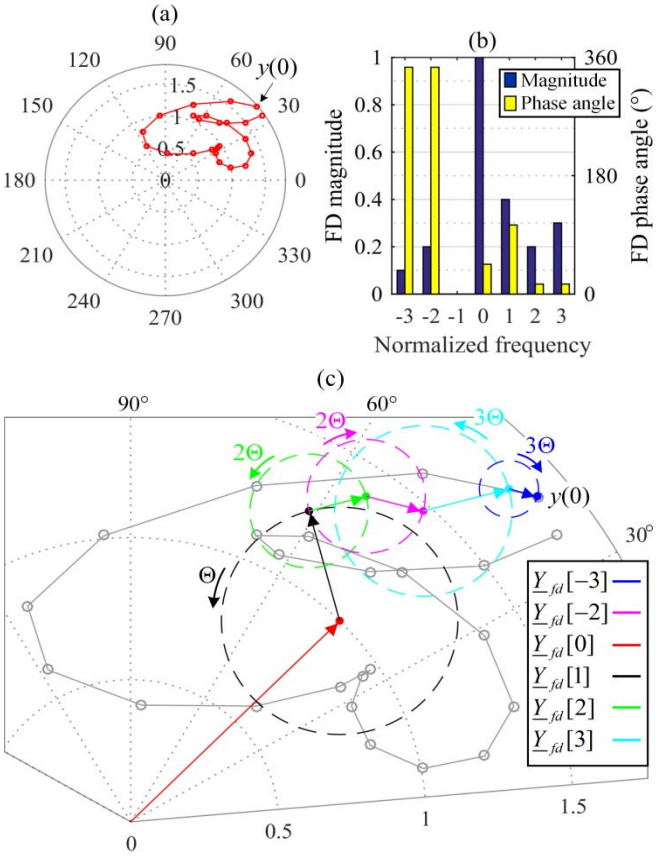

Figure 1. Closed looped object in the complex plane: (a) Polar representation; (b) FDs magnitude and phase angle vs. norm. freq.; (c) Description of FDs rotation to construct the closed looped object.

B. Simple Geometric Patterns

TABLE I. reports the parameters of the FDs for four very simple geometric patterns shown in Fig. 2.

TABLE I. SIMPLE CASES OF GEOMETRIC SHAPES PARAMETERS

Case	n	$\underline{Y}_{fd}$	Description
(a)	1		Circle centered in the origin
(b)	1	$0.4\angle 0°$	Circle centered at a specified distance
	0	$1.0\angle 45°$	
(c)	-1	$0.3\angle -45°$	Ellipse centered in the origin
	1	$0.5\angle 0°$	
(d)	-3	$0.1\angle 0°$	Double circle with different radius
	-2	$0.3\angle 0°$	
	0	$1.0\angle 45°$	

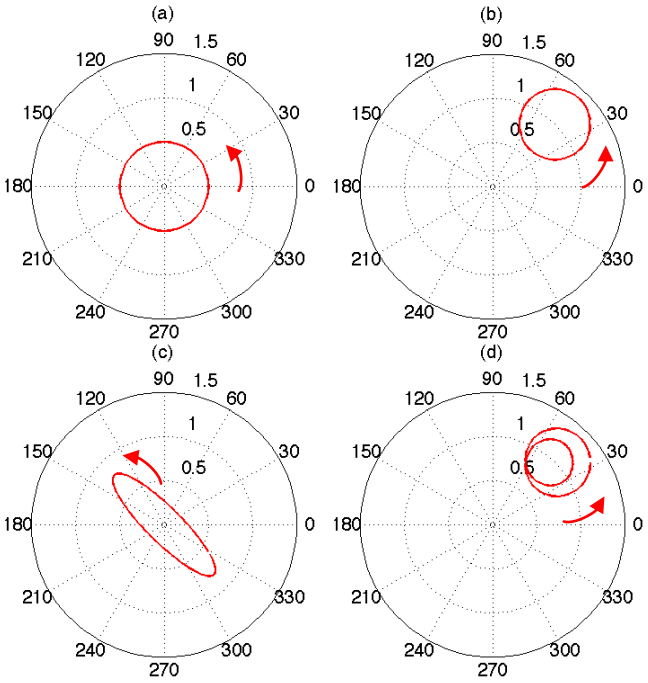

Figure 2. Simple geometric patterns representation (see Tab. I).

III. FCM APPROACH AND FDS

In steady state, the harmonic currents injected by a nonlinear load can be linearized around a reference operating point. This is represented in frequency-domain as a Norton equivalent coupled model, with the following expression:

$$\begin{bmatrix} \Delta\underline{I}_1 \\ \Delta\underline{I}_2 \\ \vdots \\ \Delta\underline{I}_H \end{bmatrix} = \begin{bmatrix} \underline{I}_1 \\ \underline{I}_2 \\ \vdots \\ \underline{I}_H \end{bmatrix} - \begin{bmatrix} \underline{I}_{\text{ref-1}} \\ \underline{I}_{\text{ref-2}} \\ \vdots \\ \underline{I}_{\text{ref-H}} \end{bmatrix} = \begin{bmatrix} \underline{Y}_{1,1} & \underline{Y}_{1,2} & \cdots & \underline{Y}_{1,K} \\ \underline{Y}_{2,1} & \underline{Y}_{2,2} & \cdots & \underline{Y}_{2,K} \\ \vdots & \vdots & \ddots & \vdots \\ \underline{Y}_{H,1} & \underline{Y}_{H,2} & \cdots & \underline{Y}_{H,K} \end{bmatrix} \begin{bmatrix} \Delta\underline{V}_1 \\ \Delta\underline{V}_2 \\ \vdots \\ \Delta\underline{V}_K \end{bmatrix} \quad (3)$$

where the vector $\underline{\boldsymbol{I}} = [\underline{I}_1, \underline{I}_2, \ldots, \underline{I}_H]^T$ represents the complex harmonic currents injected by the nonlinear load. The FCM comprises the linear gradients $\underline{Y}_{h,k}$ that relate the h^{th} harmonic current to the k^{th} harmonic voltage. The vector $\Delta\underline{\boldsymbol{V}}_k = [\Delta\underline{V}_1, \Delta\underline{V}_2, \ldots, \Delta\underline{V}_K]^T$ is the complex harmonic voltage deviation from the reference supply voltage (reference point of linearization). The vector $\underline{\boldsymbol{I}}_{\text{ref}} = [\underline{I}_{\text{ref-1}}, \underline{I}_{\text{ref-2}}, \ldots, \underline{I}_{\text{ref-H}}]^T$ is the reference harmonic current (measured for reference supply voltage). H and K are the highest harmonic orders in current and voltage to be considered.

In general, the element $\underline{Y}_{h,k}$ are complex functions of both magnitude and phase angle of $\Delta\underline{\boldsymbol{V}}_k$. For a specific condition when only one voltage harmonic variation is applied at a time and for a given phase angle, the following simple expression can be directly used:

$$\underline{Y}_{h,k} = \frac{\Delta\underline{I}_h}{\Delta\underline{V}_k} = \frac{\underline{I}_h - \underline{I}_{\text{ref-}h}}{\underline{V}_k - \underline{V}_{\text{ref-}k}}. \quad (4)$$

A systematic test and measurement procedure or set of numerical simulations can be defined to obtain the admittances $\underline{Y}_{h,k}$ for a given magnitude and for M_p evenly

spaced phase angles of the harmonic voltages $\Delta\underline{V}_k$ obtaining a sequence of complex determinations of $\underline{Y}_{h,k}(m_p)$ when the whole rotation is achieved, [9]-[15].

If the "linearity hypothesis" is fulfilled (or is assumed to be), the admittance $\underline{Y}_{h,k}$ rotates on the complex plane at twice the rate of the harmonic voltage phase angle in the clockwise direction drawing a double circle as depicted in the Fig. 3. This means that the admittance $\underline{Y}_{h,k}(0)$ can be represented as the sum of $\underline{Y}_{fd}[0]$ and $\underline{Y}_{fd}[-2]$, that are the only FDs different from zero while $\underline{Y}_{fd}[n]$ are null (or are assumed null) for all n different from 0 and -2. $\underline{Y}_{h,k}$ elements are complex numbers which R-part and I-part vary with the voltage phase angle.

Representing $\Delta\underline{V}_k$ by its Cartesian form, the phase dependency of $\underline{Y}_{h,k}$ can be modeled by means of a concise real-valued matrix which is a rank-2 tensor whose elements can be determined only using $\underline{Y}_{fd}[0]$ and $\underline{Y}_{fd}[-2]$ calculated by (1), as follows:

$$\underline{Y}_{h,k} = \begin{bmatrix} y_{1,1} & y_{1,2} \\ y_{2,1} & y_{2,2} \end{bmatrix}_{h,k}$$

$$\text{where}: \begin{cases} y_{1,1} = \Re\{\underline{Y}_{fd}[0] + \underline{Y}_{fd}[-2]\} \\ y_{1,2} = -\Im\{\underline{Y}_{fd}[0] + \underline{Y}_{fd}[-2]\} \\ y_{2,1} = \Im\{\underline{Y}_{fd}[0] - \underline{Y}_{fd}[-2]\} \\ y_{2,2} = \Re\{\underline{Y}_{fd}[0] - \underline{Y}_{fd}[-2]\} \end{cases} \quad (5)$$

Moreover, if the "linearity hypothesis" is still fulfilled (or is assumed to be) but the phase dependency of the non-linear load can be negligible, the double circle vanish and $\underline{Y}_{h,k}$ will be equal to only $\underline{Y}_{fd}[0]$ which is in turns the well known "average" admittance used in classical simplified Norton Coupled Models.

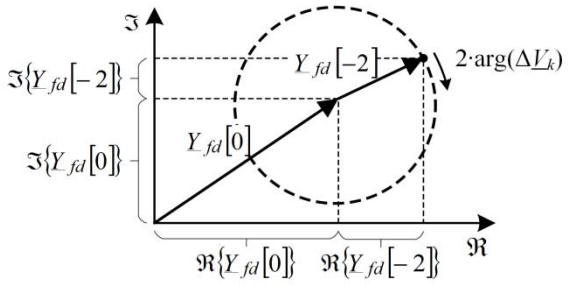

Figure 3. Phase angle dependency of the admittances $\underline{Y}_{h,k}$.

IV. FDs BASED INDEXES

Once a representation of $\underline{Y}_{h,k}$ elements based on FDs 0 and -2 is assumed, it is important to have a measure of the expected accuracy of this representation with reference to a given real specific case.

The authors here propose a "sort" of non linearity index, *NLI*, which measures the spectral content other than the components 0 and -2 for admittances and -1 and +1 for currents variations.

As for the admittances, $NLI_{Y,h,k}$, that can be seen as an index of how far the shape is different from a double circle locus, can be written as:

$$NLI_{Y,k,h} = \sqrt{\frac{\sum_{n\neq\{-2,0\}} Y_{fd}^2[n]}{Y_{fd}^2[0] + Y_{fd}^2[-2]}}\,100\,. \quad (6)$$

Concerning the current, $NLI_{\Delta I,h,k}$, that can be seen as an index of how far the shape is different from an ellipse, can be written as:

$$NLI_{\Delta I,h,k} = \sqrt{\frac{\sum_{n\neq\{-1,1\}} Y_{fd}^2[n]}{Y_{fd}^2[-1] + Y_{fd}^2[1]}}\,100\,. \quad (7)$$

A similar index can be introduced also to verify the accuracy of the applied BG voltages, where only the FD component +1 should exist. In this case, the information about the phase angles of FD(+1) should be also taken into account, which should be exactly zero.

Finally, it is worth to introduce another index, Phase Dependency Index ($PHDI_{Y,h,k}$) that, under linearity hypothesis can quantify the dependence of the device from the background phase angle:

$$PHDI_{Y,h,k} = \frac{Y_{fd}[-2]}{Y_{fd}[0]}100. \quad (8)$$

When $PHDI_{Y,h,k}$ is small enough or close to zero it means that the phase angle dependency can be negligible and "average" admittances, as commonly used in classical simplified Norton Coupled Models, can be adopted with good accuracy.

V. NUMERICAL SIMULATIONS

Two very simple circuits have been considered: a) RL Diode Rectifier, that is a circuit that reflects the circuits on which the theory of tensors was developed and b) RC Diode Rectifier that is a circuit that reflects many modern low-power devices like compact fluorescent lamps or notebook chargers. For the sake of brevity, only the effect of the background third voltage harmonic, $\Delta\underline{V}_3$, on the third harmonic current, $\underline{I}_3$, are considered in Subsection A and B for the sake of brevity while also the effects on $\underline{I}_5$,and $\underline{I}_7$ are analyzed in Subsection C It was observed that interactions among higher harmonic orders and among lower and higher harmonic orders are much more non-linear but the considerations done in this Section are still valid.

A. Single-phase RL diode rectifier

Fig. 4 shows the simulated circuit in time domain. Parameters of the simulation are: V_1=230 V; ΔV_3= [0.5%, 1-5%]*V_1 (represents up to 100% of the EN50160 limit for the third voltage harmonic, V_{3L}=5% of V_1, [16]) and $N_{\Delta\Theta}$=48 values of the phase angle; R=50 Ω and L=100 mH. The supply network is assumed to be stiff so the supplying voltage of the converter corresponds to the background voltage of the network.

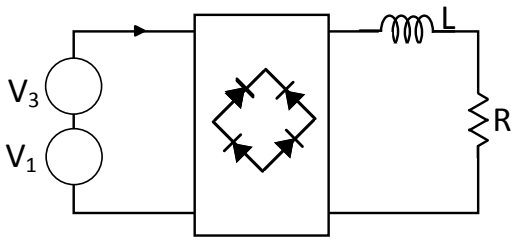

Figure 4. RL Diode Rectifier.

Fig. 5 and Fig. 6 show the polar plot (a) and the magnitude of Fourier Descriptors of ΔI_3 and of $Y_{3,3}$, respectively.

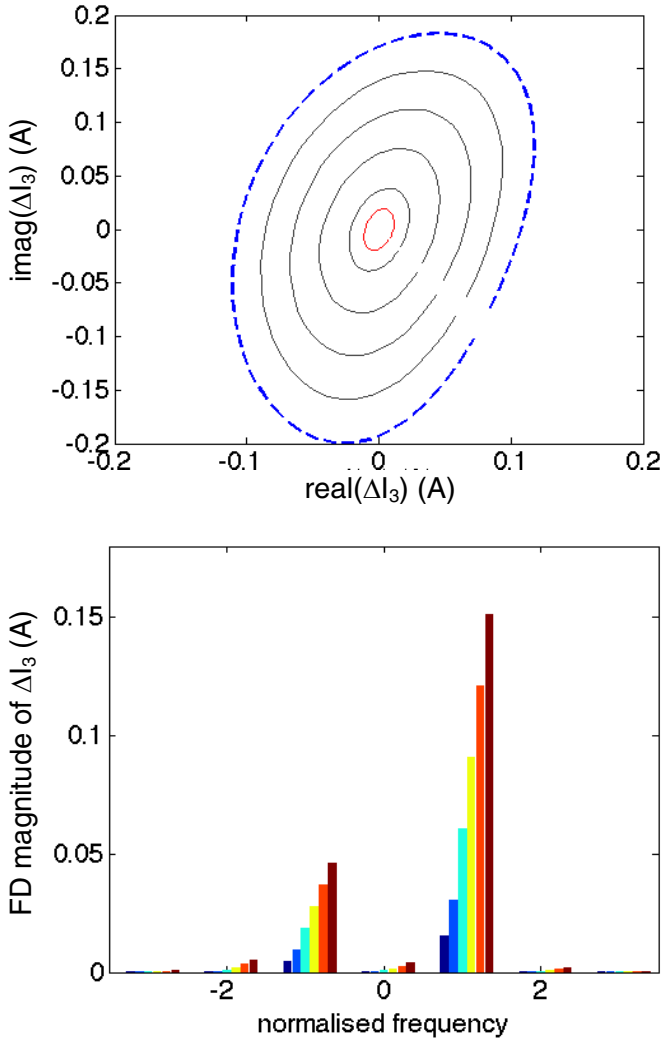

Figure 5. RL Diode Rectifier. a) Polar plot of ΔI_3, b) FDs of ΔI_3.

It is possible to observe that:

- the third harmonic current variation shows an almost elliptic shape up to background harmonic voltages value of 3% (Fig. 5 (a)) that is to say it reflects a "linear" behavior up to that value;
- the "linear" behavior is also confirmed by the FDs (Fig. 5 (b)) being the components at -1 and +1 the only frequency components different from zero up to ΔV_3=3% (yellow bars).
- when ΔV_3 becomes higher than 3% other frequency components of the FD start assuming values different from 0 that is to say that the shape is no longer a perfect ellipse even it is not visible from Fig. 5(a);
- the locus of Y_{33} is a perfect double circle Fig. 6(a) for amplitudes of ΔV_3 lower than 3% starting to show a separation between the two circles (see also Fig. 2 (d));
- this is confirmed looking at FD in Fig. 6(b).

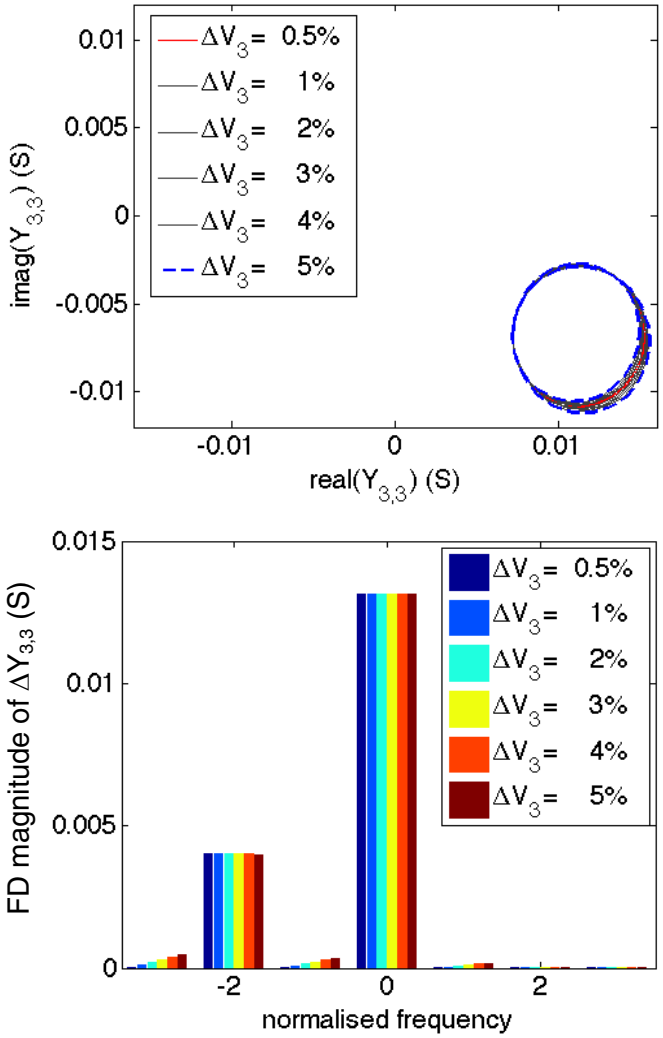

Figure 6. RL Diode Rectifier. a) Polar plot of $Y_{3,3}$, b) FDs of $Y_{3,3}$.

B. *Single-phase RC diode rectifier*

Fig. 7 shows the simulated circuit in time domain. Parameters of the simulation are: V_1=230 V; ΔV_3= [0.5%, 1-5%]*V_1 (represents up to 100% of the EN50160 limit for the third voltage harmonic, V_{3L}=5% of V_1), and $N_{\Delta\Theta}$=48 values of the phase angle have been chosen; R=100 Ω and C=1 mF.

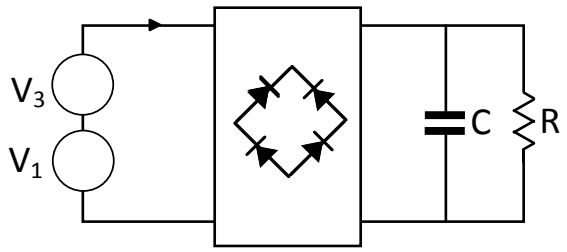

Figure 7. RC Diode Rectifier.

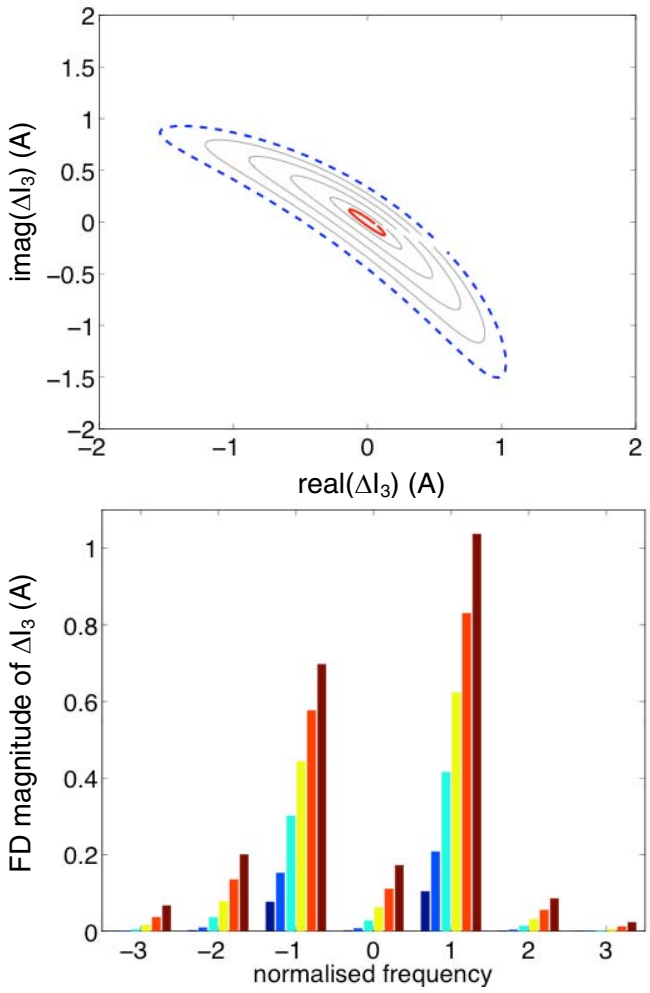

Figure 8. RC Diode Rectifier. a) Polar plot of ΔI_3, b) FDs of ΔI_3.

Figs. 8 and 9 are equivalent to Figs. 5 and 6, respectively and the following considerations can be done:

- the third harmonic current looses the elliptic shape starting from values of the background harmonic voltage higher than 1% (Fig. 8 (a));
- this can be observed mainly from Fig. 8(b) where the DC component of the FD starts to be visibly different from zero from the second group of bars (sky blue);
- the distance from the origin (that is to say the DC component of the FD in Fig. 9) seems to be independent from the BG voltage distortion magnitude, as for the RL rectifier;
- on the contrary, the -2 component starts decreasing when the "lost" of linearity starts to show;
- the RC rectifier shows a more significant non linear behavior than the RL rectifier.

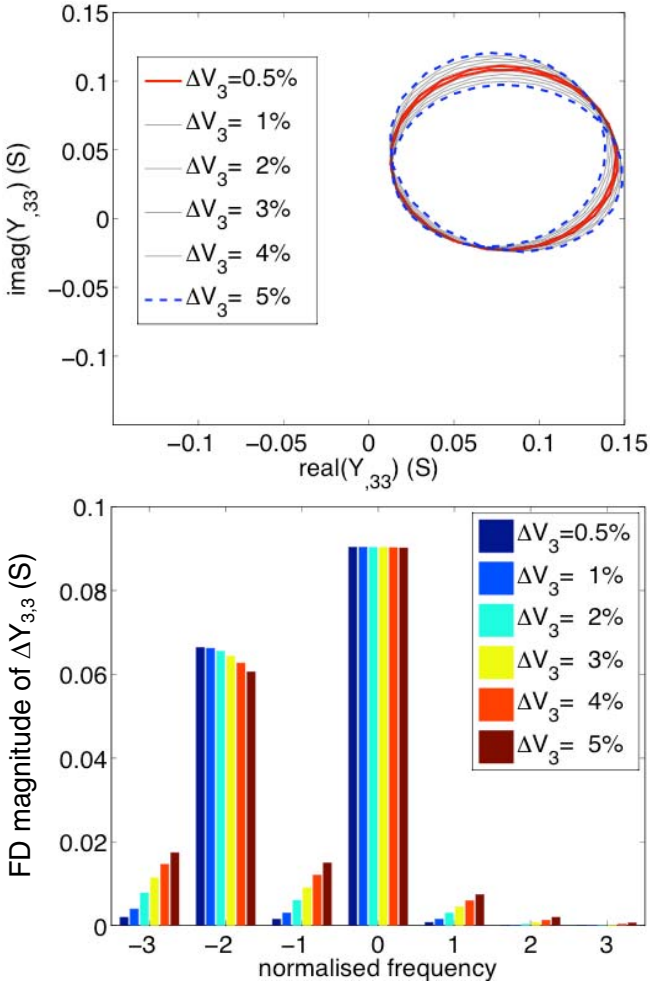

Figure 9. RC Diode Rectifier. a) Polar plot of $Y_{3,3}$, b) FDs of $Y_{3,3}$.

C. *FDs based indexes calculation and analyses*

During the numerical experiments, it was observed that $NLI_{\Delta I,h,k}$ and $NLI_{Y,k,h}$ have the same numerical values versus BG voltage magnitudes. For this reason, in what follows reference is made to the general $NLI_{h,k}$ without specifying if it refers to admittances or currents.

Fig. 10 show the non-linearity index $NLI_{h,3}$ (for h=3,5,7) for the case of the RL and RC diode rectifiers, versus the applied 3-rd BG harmonic voltage magnitude.

It is possible to observe that the non linearity index:

- is linear with the magnitude of the applied BG voltage;
- its slope is different for RL and RC rectifiers;
- in both cases, it grows with the harmonic order demonstrating that non-linearity increases with increasing distance of harmonic orders between applied BG voltage harmonic and considered current harmonic.

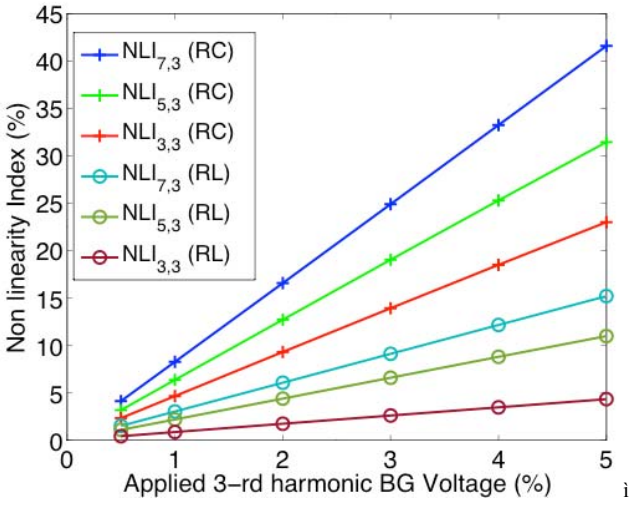

Figure 10. Non linearity index $NLI_{h,3}$ (for h=3,5,7) for the case of the RL and RC diode rectifiers, versus the applied BG ΔV_3.

In order to investigate the correlation between *NLI* and the magnitude of the errors the following error index has been introduced for each magnitude of the BG harmonic voltage:

$$\varepsilon_{\Delta I,h,k} = \frac{1}{N_{\Delta\theta}} \sum_{j=1}^{N_{\Delta\theta}} \frac{\left\| \Delta I_{h,k}^{est}(j) - \Delta I_{h,k}^{sim}(j) \right\|}{\left\| \Delta I_{h,k}^{sim}(j) \right\|} 100. \qquad (8)$$

being $\Delta I^{est}_{h,k}$ the current variation estimated by (1) for each angle variation and $\Delta I^{sim}_{h,k}$ the corresponding simulated value.

Fig. 11 shows $\varepsilon_{\Delta I,h,k}$ versus NLI for the same harmonic orders of Fig. 10. It is possible to observe, that, for both converters, the error is numerically equal to *NLI* up to 5% . This threshold can be considered as first proposal for linearity hypothesis fulfillment. This is also coherent with the values of BG distortion magnitudes corresponding to the "loss of linearity" qualitatively highlighted in the previous section for RL (3%) and RC (1%) Diode rectifiers, respectively.

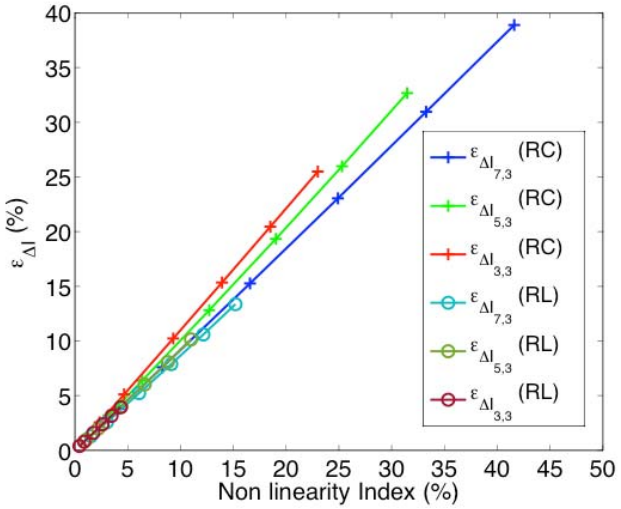

Figure 11. $\varepsilon_{\Delta I}$ versus non linearity index.

VI. Conclusions

With reference to the two simple circuits analyzed, the main outcome of the paper are:

- FDs are very good and robust tool to investigate the non linearity of PE devices;
- a threshold of the introduced NLI of 5% can be considered a good value for linearity hypothesis fulfillment accepting an error lower than 5% (errors on the entire currents will be lower of one order of quantity).

VII. References

[1] C. T. Zahn and R. Z. Roskies, "Fourier descriptors for plane closed curves," *IEEE Trans. Comput.*, vol. C-21, no. 3, pp. 269–281, 1972.

[2] Zhanwei Yuan, Fuguo Li, , Peng Zhang, Bo Chen, "Description of shape characteristics through Fourier and wavelet analysis" Chinese Journal of Aeronautics, Volume 27, Issue 1, Feb. 2014, Pages 160–168.

[3] J. Arrillaga, B. C. Smith, N. R.Watson, and A. R.Wood, Power System Harmonic Analysis. New York: Wiley, 1997.

[4] A. Medina, J. Segundo-Ramirez, P. Ribeiro, W. Xu, K. L. Lian, G. W. Chang, V. Dinavahi, and N. R. Watson, Harmonic Analysis in Frequency and Time Domain, Power Delivery, IEEE Transactions on, Vol. 28, No. 3, July 2013.

[5] J. Arrillaga, A. Medina, M. L. V. Lisboa, P. Sánchez, and M. A. Cavia, "The harmonic domain. a frame of reference for power system harmonic analysis," *IEEE Trans. Power Syst.*, vol. 10, no. 1, 1995.

[6] B.C. Smith, N.R. Watson, A.R. Wood, and J. Arrillaga. Harmonic tensor linearisation of HVDC converters. Power Delivery, IEEE Transactions on, 13(4):1244–1250, Oct 1998.

[7] Y. Sun, G. Zhang, W. Xu, and J. G. Mayordomo, "A harmonically coupled admittance matrix model for AC/DC converters," IEEE Trans. Power Syst., vol. 22, no. 4, pp. 1574–1582, 2007.

[8] J. E. Caicedo, A. A. Romero, and H. C. Zini, "Frequency domain modeling of nonlinear loads, considering harmonic interaction," in *2017 3rd IEEE Workshop on Power Electronics and Power Quality Applications, PEPQA 2017 - Proceedings*, 2017.

[9] L. Frater, "Light Flicker and Harmonic Modelling of Electrical Lighting", Ph.D. thesis in Electrical and Computer Engineering at the University of Canterbury, Christchurch, New Zealand. 2015 (http://ir.canterbury.ac.nz/handle/10092/11370).

[10] D. Gallo, C. Landi, R. Langella, M. Luiso, A. Testa, and N. Watson, "On the Measurement of Power Electronic Devices' Frequency Coupling Admittance," in *2017 IEEE International Workshop on Applied Measurements for Power Systems (AMPS)*, 2017, pp. 1–6.

[11] J. Molina, J. J. Mesas, N. Mesbahi, and L. Sainz, "LED lamp modelling for harmonic studies in distribution systems," *IET Gener. Transm. Distrib.*, vol. 11, no. 4, pp. 1063–1071, 2017.

[12] Joaquín E. Caicedo, Andrés A. Romero, Humberto C. Zini, Roberto Langella, Jan Meyer, Neville R. Watson, "Impact of reference conditions on the frequency coupling matrix of a plug-in electric vehicle charger", submitted to 18th ICHQP, May 13-16 2018, Ljubljana, Slovenia.

[13] S. Müller, J. Meyer, P. Schegner, S. Djokic: „Harmonic Modeling of Electric Vehicle Chargers in Frequency Domain", International Conference on Renewable Energies and Power Quality (ICREPQ), March 2015, La Coruna, Spain.

[14] J. Meyer, S. Müller, P. Schegner, S. Z. Djokic, A. J. Collin, X. Xu: "Comparison of Methods for Modelling Electric Vehicle Chargers for Harmonic Studies", 19th Power Systems Computation Conference (PSCC), June 2016, Genova, Italy.

[15] S. Müller, J. Meyer, P. Schegner: "Characterization of Small Photovoltaic Inverters for Harmonic Modeling", 16th ICHQP, June 2014, Bucharest, Romania.

[16] EN 50160, "Voltage characteristics of public distribution systems," 2010.